NASA TECHNICAL NOTE

NASA TN D-3233

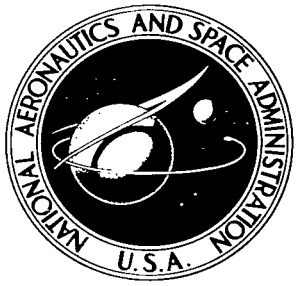

NASA TN D-3233

c. 1

0079848

TECH LIBRARY KAFB, NM

KIRTLAND AFB, N M

MINIMUM PROPELLANT CONSUMPTION ROUND-TRIP TRAJECTORIES TO MARS FOR CONSTANT-THRUST, CONSTANT-SPECIFIC-IMPULSE VEHICLES WITH OPTIMUM COASTING PERIODS

by Charles L. Zola and Laurence H. Fishbach

Lewis Research Center
Cleveland, Ohio

NATIONAL AERONAUTICS AND SPACE ADMINISTRATION • WASHINGTON, D. C. • JANUARY 1966

TECH LIBRARY KAFB, NM
0079848

MINIMUM PROPELLANT CONSUMPTION ROUND-TRIP TRAJECTORIES TO MARS FOR CONSTANT-THRUST, CONSTANT-SPECIFIC-IMPULSE VEHICLES WITH OPTIMUM COASTING PERIODS

By Charles L. Zola and Laurence H. Fishbach

Lewis Research Center
Cleveland, Ohio

NATIONAL AERONAUTICS AND SPACE ADMINISTRATION

For sale by the Clearinghouse for Federal Scientific and Technical Information
Springfield, Virginia 22151 – Price $2.00

MINIMUM PROPELLANT CONSUMPTION ROUND-TRIP TRAJECTORIES TO MARS FOR CONSTANT-THRUST, CONSTANT-SPECIFIC-IMPULSE VEHICLES WITH OPTIMUM COASTING PERIODS

by Charles L. Zola and Laurence H. Fishbach

Lewis Research Center

SUMMARY

Propellant consumption data are presented for constant-thrust, low-acceleration, Earth-Mars round-trip trajectories including escape and capture spirals at both planets. Calculations are based on a previous analysis in which the calculus of variations was applied to the problem of minimizing the propellant consumption of the round-trip trajectory treated as a single unit. Solutions given are for initial accelerations between 1.0 and 4.0×10^{-3} meter per second squared and include optimum coast phases. Results for short trip times between 340 and 460 days and a long trip time of 1000 days are presented with various wait times at Mars. Also included are examples of mission profiles where the first and/or last Earth spirals are deleted. A simple example is given showing how data of the type presented may be used for mission analysis. The mission profiles and their data are limited in scope because of computational difficulties. These results, therefore, are not sufficient for a complete study of the Mars round-trip mission.

INTRODUCTION

Electric propulsion will be attractive when it can provide lower vehicle gross weight for a space mission than can be achieved by an alternative propulsion method. Although the specific impulse of an electric rocket is high when compared with that of a chemical or nuclear rocket, propellant may still constitute a significant fraction of a given vehicle. It is thus important that the thrust vector during the long periods of propulsion be so directed as to minimize propellant requirements. This may be done by applying the calculus of variations or other optimization theory in the calculation of the trajectory.

Optimization theory has been used extensively in producing trajectory data for low-

thrust one-way trips to various planets. Some analyses have assumed a vehicle with constant power but variable thrust (refs. 1 and 2) in which the thrust vector is optimally controlled in both magnitude and direction. Others interested in the performance of constant-power electric vehicles with constant thrust, typical of state-of-the-art engines, have formulated calculus of variations solutions for these and have given examples of such trajectory solutions over a range of travel times (ref. 3). For the constant-thrust problem, the thrust and total mass flow rate are held constant at prescribed values, while the variational technique determines the optimum thrust direction programing and the placement of a coasting period (if any) to result in minimum propellant consumption.

There has been considerable interest in analyzing the use of electric propulsion in round-trip interplanetary missions. Reference 4 gives an example of the use of constant thrust but does not use optimum control of the thrust vector. Another study (ref. 5) uses the variational calculus, but for the case of variable thrust. It is the purpose of this report to present examples of short- and long-duration round trips to Mars for the constant-thrust vehicle with the thrust vector direction optimally controlled.

Many pairs of minimum propellant outbound and inbound trajectories would suffice to perform a given round trip, but total propellant requirements for the overall mission could be overestimated unless the best trajectory pair is found. The best pair was found in reference 5 by a direct trial and error method that combined precalculated one-way trajectory data into optimum round trips. In the case of constant thrust, however, the additional parameters, thrust and total mass flow rate, would require an almost prohibitive amount of precalculated data to employ a trial and error method. Therefore, the data presented in this report are based on a different approach involving a further application of the calculus of variations. The basic technique used is fully described in reference 6 where the theory developed in reference 3 for one-way trajectories is extended to the problem of optimizing the complete low-thrust round trip. Reference 6 shows that certain parameters of the variational solution relate the optimum pair of outbound and return heliocentric trajectories. The implicit relations derived in this reference are sufficient to allow the appropriate pair of trajectories to be readily identified and calculated simultaneously.

The basic computer code of reference 3 and the analytic method of reference 6 (reduced to two dimensions) were combined to provide the trajectory data of this report. An idealized circular orbit planetary model is assumed. Each round-trip trajectory is calculated straightforward from beginning to end. Every converged solution represents a minimum propellant round trip for a given thrust level and total mass flow rate. Mission time and waiting time are, however, dependent variables. External controls must be used to keep mission time and wait time constant when other parameters are varied.

Although this procedure yields accurate trajectory data, within the confines of the model, it has been found in preparing the limited amount of data for this report that cal-

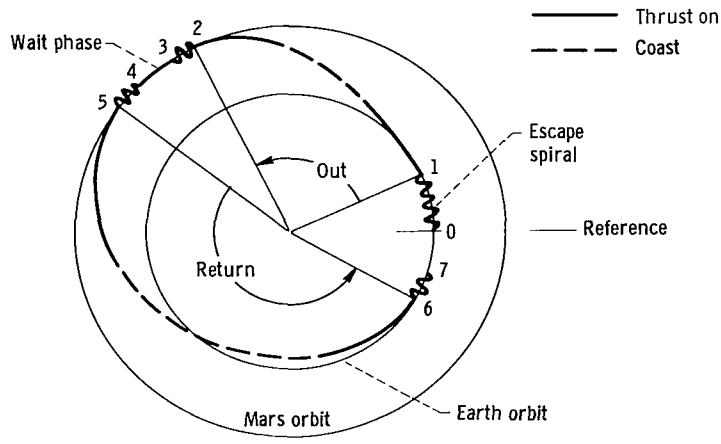

Figure 1. - Nominal mission profile for manned Mars mission using electric propulsion.

culation difficulties for certain cases can result in excessively long computation time, in many instances 20 minutes or greater on an IBM 7090. For this reason it becomes prohibitively expensive to run enough trajectory data to cover all the cases necessary for a thorough mission analysis. Nevertheless, the data presented here can be utilized in preforming examples of mission analyses employing electric propulsion (appendix B).

The chief value of the data lies in their utilization as a check on more approximate but faster trajectory schemes and as an illustration of the characteristic behavior that can be expected. For example, the trajectory method used in the mission analysis of reference 7 was initially checked by this method.

Minimum-propellant, constant-thrust, Earth-Mars round-trip trajectories are presented in the low range of trip times from 340 to 460 days with various wait times in a 1.1 Mars radii orbit. Data are also included for a trip time of 1000 days with waiting times of 300, 400, and 500 days.

It is shown in appendix B that the effects on payload of unionized propellant leaving the vehicle and inefficiencies associated with ionizing the propellant can be determined without repeating the trajectory calculations.

ANALYSIS

A typical round-trip trajectory profile to Mars is shown in figure 1. The problem model assumes a two-dimensional solar system with the planets in circular orbits about the Sun. The round-trip trajectory is approximated as a "patched" sequence of two-body planetocentric and heliocentric phases. The assumed constants of the planetary model are the following:

	Earth	Mars
Distance from Sun, m	1.495×10^{11}	2.2779179×10^{11}
Radius of planet, m	6.37123×10^{6}	3.33215×10^{6}
Gravitational constant, m^3/sec^3	3.9916661×10^{14}	0.42978661×10^{14}
Parking orbit in planet radii	1.1	1.1
Angular velocity about Sun, radians/sec	1.9909836×10^{-7}	1.0585766×10^{-7}

Heliocentric Trajectories

The heliocentric trajectories (1-2 and 5-6) in figure 1 begin and end with the vehicle in circular orbit about the Sun at each respective planet-Sun radius. During heliocentric flight, the optimal thrust vectoring program and placement of a coasting phase is governed by the variational calculus. Each trajectory is solved by using the basic computer code discussed in reference 3. The code incorporates a Runge-Kutta numerical integration technique with step size control to limit truncation error. The integration procedure is coupled with a three-variable Newton-Raphson iteration scheme to solve the boundary value problem presented by each heliocentric trajectory.

Planetocentric Trajectories

Planetocentric escape and capture phases (0-1, 2-3, 4-5, and 6-7) are included in the model because their effect on the mission as a whole can be important. Two means of executing escape and capture maneuvers are included in the model, and in this report, because their effect on the mission as a whole can be important.

The first escape method is a continuous low-thrust spiral between circular orbit at 1.1 planet radii and escape energy relative to the planet. Escape is assumed to occur sufficiently far from the planet that the vehicle can be considered out of the planet's gravity field and that it has zero velocity relative to the planet. At this point heliocentric flight begins. With long propulsion times, low-thrust planetocentric maneuvers should use optimum or close to optimum thrust vector control. Reference 8 shows that constant tangential thrust acceleration (parallel to the velocity vector) agrees within 1 percent of the variational solution. The results for constant tangential thrust are expected to likewise agree and are much easier to calculate. Even the simple tangential thrust spiral calculation would be time consuming; therefore, data from precalculated generalized tangential spiral solutions (ref. 4) have been fitted within 1-percent accuracy by empirical

curves. In this way, time and propellant requirements for escape or capture spirals can be found for any given pair of thrust and total mass flow rate.

The second maneuver used a parabolic conic section to replace the low-thrust spirals necessary when electric thrustors are employed for planetocentric escape or capture. To escape, it is assumed that a high-thrust booster places the vehicle on an escape parabola. No penalty for performing this high-thrust maneuver has been included in the data of this report. The vehicle coasts until it can be assumed that it is in heliocentric space having zero velocity relative to the planet. The time spent coasting on this parabola has not been included in the mission time. At this point the electric thrustors are turned on and the heliocentric transfer begins. The use of parabolic capture trajectories represents high-thrust braking into elliptic or circular orbits or atmospheric braking followed by descent to the surface of the planet.

Calculation of Complete Trip

Combining the results of the planetocentric maneuvers with the calculus of variations solution to the heliocentric transfer yields the complete vehicle performance. The mass at any time M, the thrust F, and the total mass flow rate $\dot{M}_{TOT}$ are sufficient to calculate both the trajectory and accompanying mass change.

The $\dot{M}_{TOT}$ is assumed to be inclusive of all mass flow rates regardless of whether or not they contribute to thrust. In presenting the results of this report, it has been found to be advantageous to use alternate parameters that are defined in terms of $\dot{M}_{TOT}$ and F. These parameters are the thrust to initial mass ratio (initial acceleration) F/M_0 and the effective power to initial mass ratio P/M_0. The F/M_0 ratio is defined by the thrust and initial mass, and P/M_0 can be expressed as

$$\frac{P}{M_0} = \frac{1}{2}\left(\frac{F}{M_0}\right)\frac{F}{\dot{M}_{TOT}} \tag{1}$$

where $F/\dot{M}_{TOT}$ is the effective exhaust velocity of the expelled mass. The P/M_0 is shown in appendix B to be a useful parameter in that it is of the order of the actual beam power and total propulsive power required by the vehicle and differs only by thrustor efficiency functions.

When P/M_0 and F/M_0 are used, the calculation of a typical round-trip trajectory commences with arbitrarily choosing an initial mass M_0 and thus defining F and $\dot{M}_{TOT}$. The M_0 is identical to M_1 when the initial Earth spiral is replaced by a high-thrust maneuver. The mass change evaluated for each phase then determines the initial mass of each succeeding phase. The process is repeated throughout the trajectory and

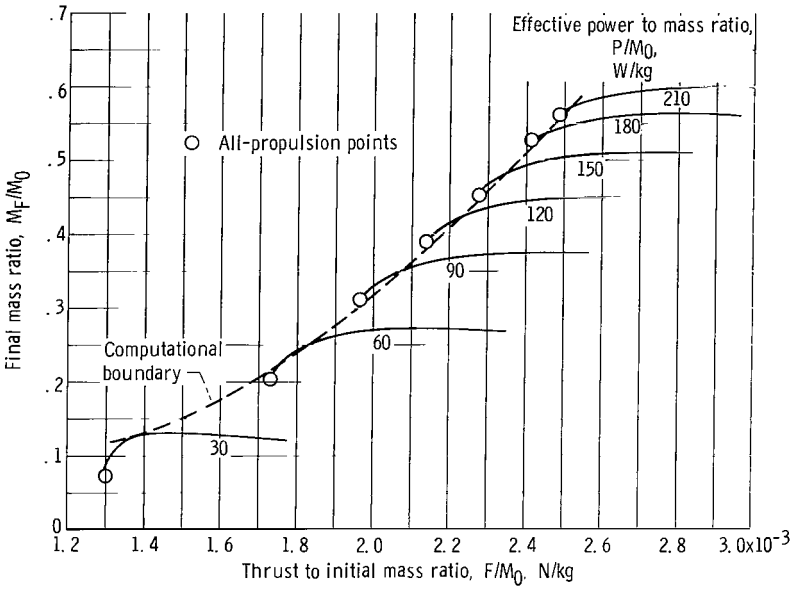

Figure 2. - Final mass ratio against thrust to initial mass ratio. Mission time, 380 days; wait time, 10 days; four spirals.

finally results in a terminal mass fraction referred to as M_F/M_0. The final mass M_F corresponds to M_6 for no terminal spiral or to M_7 when a terminal spiral is included.

The trajectory calculations presented here do not include arbitrary (i. e., nonpropellant) mass changes at Mars. In any actual round-trip mission, some arbitrary amount of mass (e. g., the landing and exploration system) might be jettisoned or left behind at the start of the return trip. Final mass fraction of the trip M_F/M_0 decreases as the fraction of jettisoned mass to initial spacecraft mass increases.

RESULTS AND DISCUSSION

Trajectory data are presented in the form of graphs (hereafter called performance maps), such as figure 2, showing final mass ratio M_F/M_0 as a function of thrust to initial mass ratio F/M_0. At each point on a map an effective specific impulse (effective jet velocity divided by the gravitational constant of Earth, 9.80665 m/sec^2) is defined since the power to mass ratio is directly proportional to the thrust to mass ratio and jet velocity (eq. (1)).

Performance maps are presented for three classes of missions: short mission times with four spirals, short mission times with the initial and/or final Earth spirals omitted, and a long, four-spiral mission time with various waiting times at Mars.

All the performance maps presented in this report (appendix C) have similar characteristics. The purpose of this section is to examine general changes in performance

brought about by changing the mission parameters, such as mission time and waiting time, and changing the profile by the omission of spirals.

Figure 2 is typical of the performance maps, in this case a four-spiral trip for a 380-day total mission time with a 10-day wait at Mars. Along each constant P/M_0 line there exists an optimum F/M_0, which yields a maximum M_F/M_0. The M_F/M_0 continues to improve in the direction of higher P/M_0. For finite F/M_0, as P/M_0 becomes infinite (infinite specific impulse), the mass ratio approaches unity.

In figure 2, the circled point at the extreme left of each P/M_0 curve is where the round-trip trajectory degenerates into all propulsion on both legs of the trip. For each P/M_0 this point defines the lower bound on F/M_0. All-propulsion, or zero coast time, solutions result when the energy requirements are so severe that the thrustor must operate continuously over the available time. To the right of the all-propulsion point at each P/M_0 some coasting occurs on both outbound and inbound legs.

Examination of a typical P/M_0 line shows that as F/M_0 is decreased (heading towards the all-propulsion point), M_F/M_0 starts to decrease rapidly. As was pointed out in the INTRODUCTION, computational difficulties arise when certain cases are run; typical of these are those near the all-propulsion boundary. Therefore, to save computation time, solutions were usually stopped before the all-propulsion points were reached. The dashed line in figure 2 represents the F/M_0 where the solution would have normally been terminated.

The sketch shows that as F/M_0 is decreased, both outbound and return coast times approach zero. The outbound coast time tends to level off until the return coast time is short, then both appear to approach zero simultaneously. This is the area of computational difficulty mentioned previously. Solutions were stopped at an F/M_0 that corresponds to about a 5-day outbound coast (indicated by dashed line).

The bound that appears on the left-hand side of the performance maps (appendix C) represents the F/M_0 where solutions were stopped and the data should not be extrapolated to lower F/M_0.

Figure C1(a) in appendix C presents a plot of a round-trip trajectory for a 30-day wait, 380-day trip with no initial or final Earth spirals. Figure C1(b) presents a similar plot for a 400-day wait, 1000-day trip with four spirals. Table CI in appendix C gives trajectory variables as functions of time for the 380-day trip. The purpose of presenting these data in this manner is to allow the reader to check any results he has obtained with his own trajectory program against those presented here.

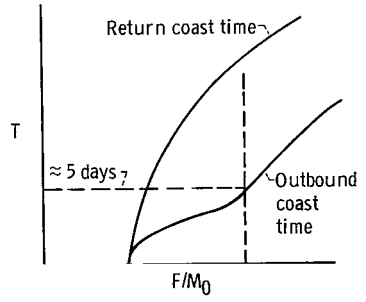

The remainder of this report will be concerned with the effects of trip time, wait time, and mission profile on final mass ratio. These effects will be shown by plotting maximum

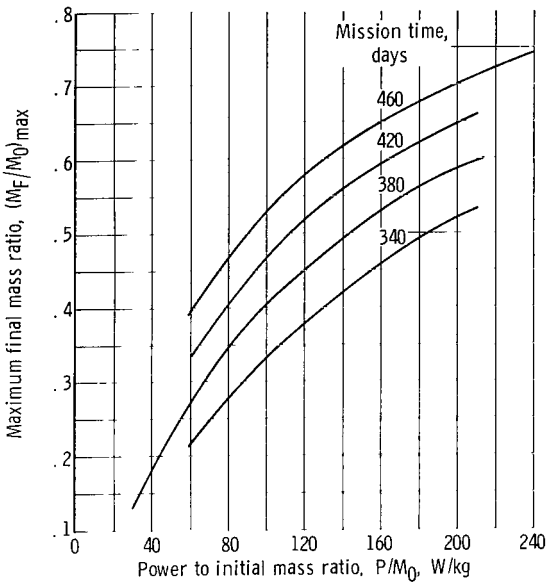

Figure 3. - Effect of mission time on maximum final mass ratio. Four-spiral missions; wait time, 10 days.

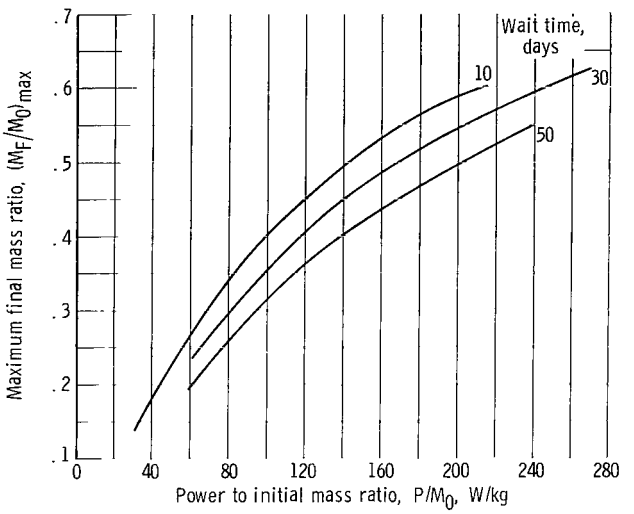

Figure 4. - Effect of wait time on maximum final mass ratio. Four-spiral missions of 380 days.

M_F/M_0 against P/M_0 as determined from the appropriate performance maps found in appendix C.

Four Spiral Trips

Figure 3 shows the effect of trip time on final mass fraction for trips with a constant wait time. The performance maps for trip times of 340, 380, 420, and 460 days with a 10-day wait are shown in figure C2 of appendix C. As trip time is increased from 340 to 460 days, the final mass fraction can be seen to increase from 0.441 to 0.634 at a P/M_0 of 150 watts per kilogram. Longer trip time allows lower acceleration and, hence, higher specific impulse at the same power, which results in increased M_F/M_0.

Figure 4 shows the effect of wait times of 10, 30, and 50 days on final mass fraction for a 380-day trip. Figure C3 shows the performance maps for these missions. It can be seen in figure 4 that M_F/M_0 decreases with increasing wait time dropping from 0.511 at a 10-day wait to 0.417 at a 50-day wait for P/M_0 of 150 watts per kilogram. For a fixed mission time and an increasing wait time, this decrease in M_F/M_0 is a result of forcing the transfer time to be shorter, which results in an effectively more difficult mission. The optimum wait time is therefore zero days, but the choice of wait time is not arbitrary and will be dictated by the time required to complete the objectives of the mission.

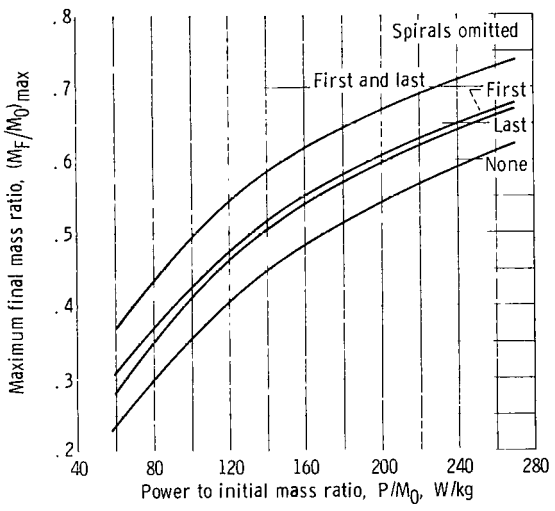

Figure 5. - Effect of omission of spirals at Earth on maximum final mass ratio. Mission time, 380 days; wait time, 30 days.

Omission of First and/or Last Spirals

Maps are presented in appendix C (figs. C4 and C5) for 340- and 380-day trip times, respectively, with a 30-day wait in which one or two spirals have been omitted. Omission of the first spiral corresponds to a boost of the electric vehicle to escape energy through another type of rocket. Figure 5 shows the effect on final mass fraction of removal of the first spiral for the 380-day mission. The M_F/M_0 can be seen to increase from 0.467 to 0.534 at a P/M_0 of 150 watts per kilogram. The actual change in mass ratio must take into account the boost vehicle requirements of the no-initial-spiral trip, since for this case M_0 is no longer the initial mass leaving the Earth orbit.

Omission of the terminal spiral is accomplished by assuming that the returning vehicle can either be captured in a high energy ellipse or use atmospheric braking to the surface from an entry velocity equal to escape velocity $\left(\sqrt{2}\, V_{circular} \approx 11\,200 \text{ m/sec}\right)$. For a mission analysis using this profile, provisions must be made for landing the men, such as including a reentry capsule in the payload or picking up the crew in the high energy ellipse with a separate Earth-launched craft. Figure 5 shows the effects of omitting the final spiral for the 380-day mission. The M_F/M_0 increases from 0.467 to 0.523 at 150 watts per kilogram. Omission of the last spiral allows more time (of the order of 20 days) for the heliocentric transfers, hence higher M_F/M_0.

Eliminations of both the first and last spirals could be brought about by a boost to escape energy at the start of the mission and atmospheric reentry from escape energy at Earth return. In figure 5, M_F/M_0 is seen to increase from 0.467 to 0.600 at a P/M_0 of 150 watts per kilogram, when both Earth spirals are omitted. Again, a boost vehicle must be taken into account and a reentry vehicle included in the payload.

One-Thousand-Day Trip Time

Figure C6 presents maps for 1000-day trips with wait times of 300, 400, and 500 days. Figures 6(a) and (b) show how the final mass ratio increases with decreasing wait time. In figure 6(a) the maximum final mass had been recorded at each P/M_0 by finding the best F/M_0. Along each dashed curve in figure 6(b), however, P/M_0 and F/M_0 are

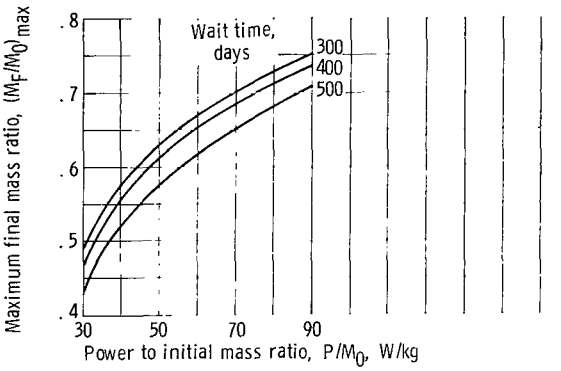

(a) Optimum thrust to initial mass ratio.

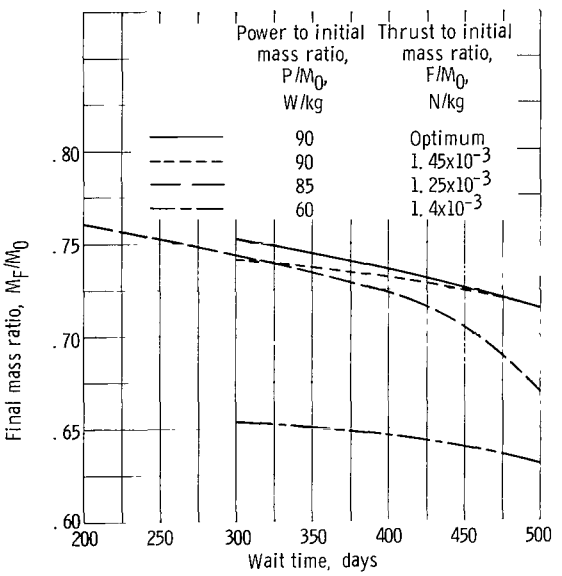

(b) Thrust to mass ratio held constant.

Figure 6. - Effect of wait time for 1000-day 4-spiral trip.

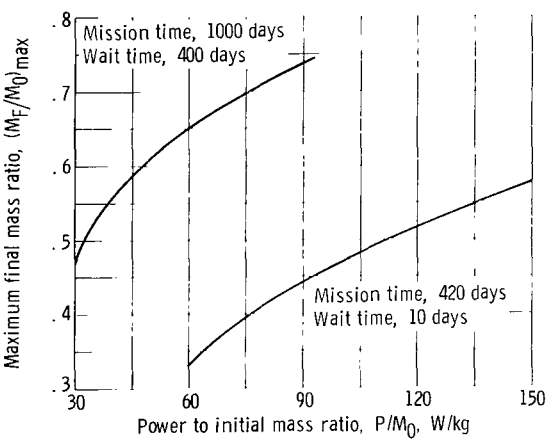

Figure 7. - Long against short mission times. Maximum final mass ratio; four-spiral missions.

held constant at different arbitrary values. The solid curve, for contrast, has P/M_0 fixed at 90 watts per kilogram, but the optimum (highest M_F/M_0) value of F/M_0 has been found at each wait time. Calculation difficulties were too great to allow extension of the data below 200 days of wait for each P/M_0 and F/M_0 pair.

Decreasing wait time for a fixed mission time forces the heliocentric portions of the trip to use higher elapsed times and travel angles. The need for return leg travel angles greater than $3\pi/2$ radians contributes to the difficulties mentioned previously. The propellant consumption of low-thrust vehicles usually decreases with increasing heliocentric time. It is therefore probable for any fixed pair of P/M_0 and F/M_0 that M_F/M_0 will continue to increase until wait time equals zero.

The data presented in figures 6(a) and (b) are in direct contrast with the so-called impulsive Hohmann round trip. When impulsive trajectories are used with the stipulation that the velocity pulses must occur at the beginning and end of each trajectory, ΔV must increase if the travel time on a leg is found to be greater than the Hohmann time (260 days). Therefore, for a 1000-day mission, impulsive trips have an optimum wait time of about 450 days while it appears that low-thrust trips have an optimum of zero days. It might be advisable, however, to stay at Mars for the longer wait times presented in the maps in order to do extensive investigation of the planet and avoid exposing the astronauts to the hazards of heliocentric transfer for an unnecessarily long time.

Figure 7 compares $\left(M_F/M_0\right)_{max}$ for a 1000-day trip with a 400-day wait and a 420-day trip with a 10-day wait. In general, longer

trips will allow the use of lower P/M_0, to result in the same final mass fraction, or will yield higher M_F/M_0 values at the same P/M_0. Since powerplant fraction is proportional to P/M_0, increasing trip time appears, as expected, to benefit payload capability. For $P/M_0 = 90$ watts per kilogram, the long trip time yields $\left(M_F/M_0\right)_{max} = 0.735$ as opposed to 0.441 for the short trip time.

CONCLUDING REMARKS

Performance maps have been presented for constant low-thrust round-trip missions of short and long duration. For simplicity, it is assumed that no mass change occurred at Mars. It has been found that generation of these maps by the method used herein is very time consuming and would be far too costly to provide the large amount of trajectory data needed in extended mission analysis. The problem cases were those that (1) were near the all-propulsion boundary or (2) had travel angles on the return leg greater than $3\pi/2$ radians, which is typical for trip times above 500 days with a waiting time of the order of 10 days and for 1000-day missions where the wait time is below 200 days. If, in the future, further improvements can be made in the methods of solving the variational trajectory problem for constant thrust, the computing time element may be of less concern. The maps are extremely useful as a basis for checking more approximate solutions to the trajectory problem.

Since each point on a map represents an optimum round trip in terms of maximizing final mass ratio for a given P/M_0 and F/M_0, there is no need to piece together one-way trips through a trial and error search.

For constant-thrust trajectories, the all-propulsion boundary represents an important limitation on the area of valid solutions, that is, continuous thrusting on both legs of the heliocentric transfers.

As opposed to high-thrust solutions, final mass ratio of low-thrust solutions increases monotonically with increasing mission time.

A high-thrust, Hohmann-type round trip to Mars possesses an optimum waiting time (about 450 days) at a mission time of approximately 1000 days. It is interesting to note that this characteristic of high-thrust trajectories does not appear in the case of low thrust. For both the 1000-day missions and the short missions presented herein, final mass is seen to improve with decreasing wait time.

Also shown was that a change in mission profile from the four-spiral trip may result in improved vehicle performance. The four-spiral mission (as shown in appendix B) requires a low value of specific powerplant mass α to be competitive with nuclear or chemical rockets at short mission times. For high α, other mission profiles such as boosting beyond escape energy and reentry from hyperbolic velocity were studied with

approximate techniques in reference 7 and were shown to improve the competitive position of electric propulsion. Reference 7, whose trajectory solutions were checked against accurate performance maps, contains a more complete study of the effect of mission profile. This report does not contain accurate solutions to these other profiles because of the prohibitive cost of obtaining them.

Lewis Research Center,
National Aeronautics and Space Administration,
Cleveland, Ohio, September 24, 1965.

APPENDIX A

SYMBOLS

e	eccentricity of vehicle trajectory
F	thrust, N
g	gravitational constant of Earth, 9.80665, m/sec^2
I_{SP}	specific impulse of thrustor, sec
K	switching function (see ref. 3)
ℓ	semilatus rectum of vehicle trajectory, m
M	mass of vehicle, kg
M_F	final mass of electric vehicle, kg
M_L	useful payload mass of electric vehicle, kg
M_P	mass of electric vehicle propellant, kg
M_{PP}	mass of electric vehicle powerplant, kg
$\dot{M}_{TOT}$	total mass flow rate
M_0	initial mass of electric vehicle, kg
P	effective jet power, W
P_T	total power output of powerplant, W
R	distance of vehicle from Sun, m
T	elapsed time, sec
V	velocity
α	specific powerplant mass, kg/W
η	overall engine efficiency
η_P	power efficiency of engine
η_u	fraction of mass leaving vehicle providing thrust
θ	true anomaly of vehicle trajectory, radians
$\lambda_1, \lambda_2, \lambda_3, \lambda_4, \lambda_5$	Lagrangian multipliers in calculus of variations solution (see ref. 3)
φ	elapsed travel angle, radians
ψ	thrust angle relative to local horizontal, radians
ω	argument of pericenter, angle measured from starting point of each trajectory to pericenter radius in the direction of motion, radians

APPENDIX B

USE OF PERFORMANCE MAP FOR MISSION ANALYSIS

The simplest concept of an electric vehicle is that it consists of three integral parts, propellant, powerplant, and payload. If this is the case and if a fixed payload and structure are assumed, the difference between the initial mass M_0 and the final mass M_F can be regarded as the propellant M_P necessary to fly the mission:

$$M_P = M_0 - M_F \tag{B1}$$

The powerplant mass M_{PP} is related to the total power output P_T by the specific powerplant mass α:

$$M_{PP} = \alpha P_T \tag{B2}$$

The payload M_L is then the initial mass minus the propellant and powerplant masses:

$$M_L = M_0 - M_P - M_{PP} \tag{B3}$$

or in terms of M_F and αP_T,

$$M_L = M_F - \alpha P_T \tag{B4}$$

Normalizing equation (B4) with respect to M_0 yields

$$\frac{M_L}{M_0} = \frac{M_F}{M_0} - \alpha \frac{P_T}{M_0} \tag{B5}$$

In this simple analysis, when inefficiencies in the thrustor are ignored, P_T/M_0 is equivalent to P/M_0 appearing as a parameter on the performance maps. Figure 8 is a typical performance map showing one line of constant P/M_0. Since the performance map presents M_F/M_0 along lines of constant P/M_0, M_L/M_0 can readily be obtained. This process is illustrated in figure 8 where α has been taken to be 3×10^{-3} kilogram per watt. When thrustor inefficiencies are ignored, $\alpha P/M_0$ is constant along a P/M_0 line and the M_L/M_0 line is vertically displaced by a uniform amount below the M_F/M_0 line; hence, maximum M_F/M_0 gives maximum M_L/M_0.

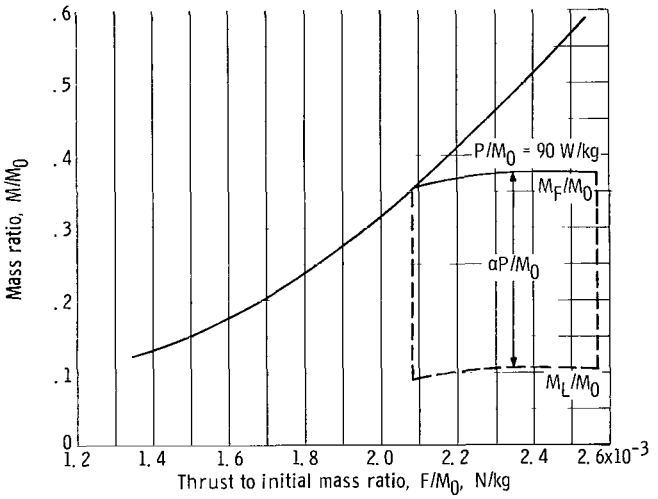

Figure 8. - Final and payload mass ratios against thrust to initial mass ratio. Mission time, 380 days; wait time, 10 days; specific powerplant mass, 3.0×10^{-3} kilogram per watt; effective power to mass ratio, 90 watts per kilogram.

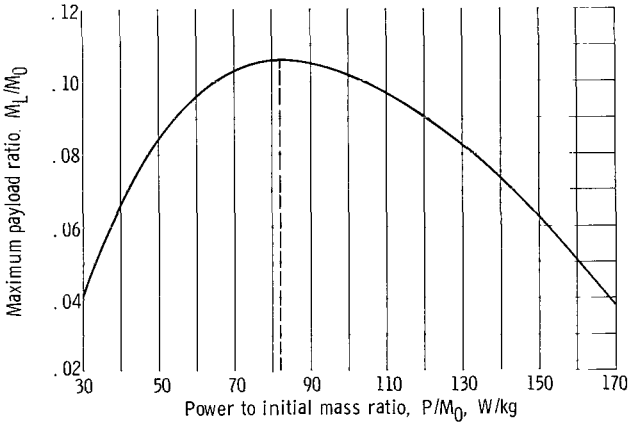

Figure 9. - Maximum payload ratio at each power to mass ratio. Mission time, 380 days; wait time, 10 days; specific power plant mass, 3.0×10^{-3} kilogram per watt.

Repeating this process for all P/M_0 on the full map (fig. C2(b)) and then plotting maximum M_L/M_0 against P/M_0 yield the overall maximum M_L/M_0 and optimum P/M_0. This is illustrated in figure 9.

To determine the optimum thrust to mass ratio F/M_0, one plots the F/M_0 that gives maximum M_L/M_0 at each P/M_0 against P/M_0 and from the optimum P/M_0 determines optimum F/M_0.

Optimum specific impulse I_{SP} is then found from the optimum values of P/M_0 and F/M_0 from the relation

$$I_{SP} = \frac{2\frac{P}{M_0}}{\frac{F}{M_0}g} = \frac{F}{\dot{M}_{TOT}g} \qquad \text{(B6)}$$

It should be noted that the optimized parameters are for a fixed value of α, and an entirely new set would be found by repeating the procedure just followed for a new α.

Figure 10 shows optimum specific impulse, thrust to mass ratio, power to mass ratio, and maximum payload fraction as a function of α for a 380-day, 10-day wait, four-spiral mission. The I_{SP}, F/M_0, and P/M_0 are all seen to decrease with increasing α, and M_L/M_0 rapidly approaches zero.

Having a set of performance maps for different trip times but constant wait time is thus sufficient to determine payload ratio against trip time over a range of α.

The specific impulse of the thrustor $I_{SP,\,ENG}$ is defined as the ratio of thrust to weight flow rate of ions contributing to thrust. If η_u represents that fraction of mass leaving the vehicle which is providing thrust (the propellant utilization efficiency), $I_{SP,\,ENG}$ may be expressed as

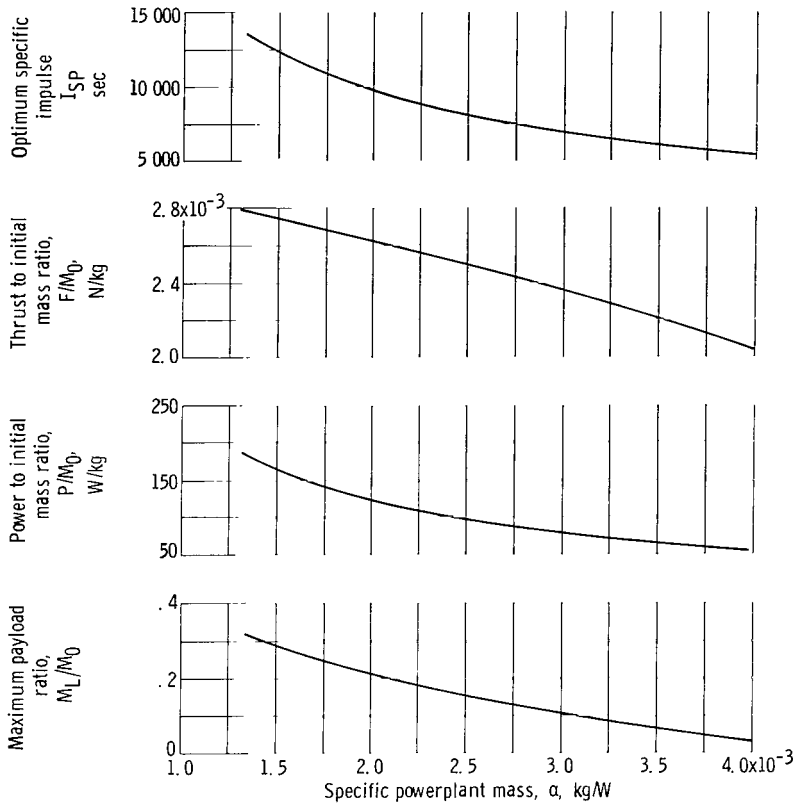

Figure 10. - Optimum specific impulse, thrust to initial mass ratio, power to initial mass ratio, and maximum payload ratio against specific powerplant mass. Mission time, 380 days; wait time, 10 days.

$$I_{SP,\,ENG} = \frac{F}{\eta_u \dot{M}_{TOT} g} = \frac{2\,\frac{P}{M_0}}{\eta_u \frac{F}{M_0} g} \tag{B7}$$

For electric thrustors, the power efficiency of the engine η_P can be presented as in the sketch as a function of the specific impulse of the thrustor.

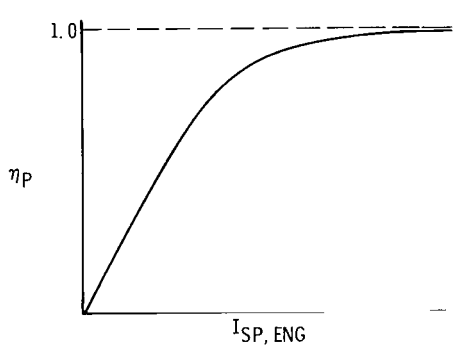

If η_u is known, it is possible at each point on the map to determine the overall engine efficiency η ($\eta = \eta_u \eta_P$) and the total power requirements when efficiency is taken into account:

$$\frac{P_T}{M_0} = \frac{1}{\eta_u \eta_P}\left(\frac{P}{M_0}\right) \tag{B8}$$

where $\eta_P = \eta_P(I_{SP,\,ENG})$.

Equation (B8) may not be of interest if a detailed study of the effect of the individual efficiencies η_u and η_P is not required. A more simple analysis, showing the effect of overall efficiency, can be made when the variation of η is known or can be assumed for an electric thrustor system directly as a function of $F/\dot{M}_{TOT}$. In this case,

$$\frac{P_T}{M_0} = \frac{1}{\eta}\left(\frac{P}{M_0}\right) \tag{B9}$$

where $\eta = \eta(F/\dot{M}_{TOT}) = \eta(I_{SP})$, and I_{SP} is given by equation (B6).

Thus, at each point on the map the total power requirements are given, and the effects of efficiency can be determined without the need for recomputing the trajectories since F was interpreted as total thrust and $\dot{M}_{TOT}$ as all the mass leaving the vehicle.

A further discussion of the effects of efficiency, structure, boosting, atmospheric braking, etc., on payload fraction is beyond the scope of this report. References 7 and 9, which are concerned with mission analysis, more fully treat this subject. The data of reference 9 were generated with a one-way calculus of variations program similar to the round-trip program employed here.

APPENDIX C

PERFORMANCE MAPS

This appendix presents more detailed data on the performance of the constant-thrust, constant-specific-impulse vehicle for the Mars round-trip mission.

Table CI presents a time history of the vehicle trajectory for a 380-day, 30-day-wait mission with no initial or final Earth spirals.

Figure C1(a) is a polar coordinate plot of this trajectory. Figure C1(b) plots the trajectory for a 1000-day four-spiral trajectory with 400 days of wait.

Figures C2 and C3 are performance maps for short mission time, four-spiral missions, with various wait times at Mars.

Figures C4 and C5 are maps for short mission times where the initial and/or terminal Earth spirals have been deleted.

Figure C6 presents data for a 1000-day, four-spiral mission for three different waiting times at Mars.

TABLE CI. - TRAJECTORY VARIABLES AS FUNCTION OF TIME FOR 380-DAY TRIP

[Thrust to initial mass ratio, F/M_0, 2.2555×10^{-3} N/kg; effective power to mass ratio, P/M_0, 100 W/kg; Lagrangian multiplier, λ_4, 267.93; constant of integration, 1.9229×10^{-4}.]

(a) Outbound leg

Elapsed time, T, sec	Elapsed travel angle, φ, radians	Distance of vehicle from Sun, R, m	Mass of vehicle, M, kg	Thrust angle relative to local horizontal, ψ, radians	Switching function, κ	Lagrangian multipliers in calculus of variations solution				Semilatus rectum of vehicle trajectory, ℓ, m	Eccentricity of vehicle trajectory, e	True anomaly of vehicle trajectory, θ, radians	Argument of pericenter, ω, radians
						λ_1	λ_2	λ_3	λ_5				
0	0	1.4950×10^{11}	1000.0	0.6386	5.4623	4.3441×10^{-2}	5.8518×10^{-3}	2.5836×10^{-8}	1.0000	1.4950×10^{11}	0	0	0
1.7280×10^{5}	.03458	1.4952	995.60	.6613	5.2045	4.2976	5.5227	2.5060	1.0280	1.5264	.02249	.3822	-.3476
6.9120	.14023	1.4988	982.42	.7361	4.4364	4.1232	4.5510	2.2683	1.1065	1.6198	.09044	.4667	-.3264
1.3824×10^{6}	.28429	1.5121	964.84	.8525	3.4358	3.7965	3.3186	1.9509	1.1983	1.7401	.18129	.5884	-.3042
2.0736	.42947	1.5380	947.25	.9893	2.4779	3.3506	2.2023	1.6547	1.2753	1.8510	.27072	.7202	-.2908
2.7648	.57248	1.5788	929.67	1.1500	1.5736	2.7861	1.2467	1.4048	1.3377	1.9453	.35651	.8618	-.2893
3.4560	.70981	1.6360	912.09	1.3458	.7259	2.1172	.4846	1.2196	1.3855	2.0124	.43574	1.0144	-.3046
4.0903	.82795	1.7033	895.95	1.5920	0	1.4314	-.0304	1.1128	1.4169	2.0349	.49868	1.1698	-.3418
Coast													
6.3833	1.1804	1.9868	895.95	1.5920	0	-1.3288	-.5343	1.1038	1.4169	2.0349	.49868	1.5222	-.3418
6.7789	1.2247	2.0293	887.16	-1.8236	.3828	-1.7593	-.4545	1.1333	1.4334	1.9926	.46112	1.6100	-.3853
7.4201	1.3072	2.1051	869.58	-1.6455	1.2027	-2.6218	-.1961	1.2035	1.4783	1.9485	.39162	1.7619	-.4548
8.1113	1.3840	2.1676	852.00	-1.5178	2.0889	-3.4844	.1848	1.2868	1 5426	1.9462	.32444	1.8909	-.5070
8.8025	1.4572	2.2161	834.42	-1.4150	3.0444	-4.3446	.6825	1.3836	1.6291	1.9793	.25514	2.0028	-.5456
9.4937	1.5286	2.2504	816.83	-1.3265	4.0757	-5 1989	1.2959	1.4957	1.7406	2.0451	.18037	2.1013	-.5726
1.0185×10^{7}	1.5997	2.2709	799.25	-1.2469	5.1898	-6.0418	2.0281	1.6268	1.8807	2.1426	.09742	2.1896	-.5899
1.0717	1.6551	2.2775	785.72	-1.1896	6.1089	-6.6780	2.6766	1.7436	2.0103	2.2394	.02651	2.2525	-.5974
1.0904	1.6748	2.2779	780.97	-1.1700	6.4444	-6.8973	2.9223	1.7885	2.0607	2.2779	0	2.3846	-.7098
1.1906	1.7809	2.2779	755.47	Spiral									
Wait at Mars													

(b) Return leg

1.4501×10^{7}	2.0556	2.2779×10^{11}	755.47	Spiral									
1.5469	2.1581	2.2779	730.84	-2.1244	6.4444	-6.0663×10^{-2}	-3.7493×10^{-3}	-1.5067×10^{-8}	2.2079	2.2779×10^{11}	0	-3.1416	3.1416
1.5642	2.1763	2.2775	726.45	-2.1094	6.1897	-5.9421	-3.5506	-1.4676	2.2595	2.2257	.02960	-2.4469	2.4651
1.6160	2.2298	2.2713	713.26	-2.0640	5.4373	-5.5591	-2.9879	-1.3591	2.4087	2.0788	.11462	-2.4033	2.4749
1.6851	2.2991	2.2504	695.68	-2.0014	4.4626	-5.0314	-2.3111	-1.2318	2.5946	1.9057	.21946	-2.3433	2.4842
1.7543	2.3673	2.2135	678.10	-1.9347	3.5217	-4.4931	-1.7113	-1.1200	2.7653	1.7598	.31517	-2.2790	2.4882
1.8234	2.4358	2.1592	660.51	-1.8615	2.6164	-3.9514	-1.1823	-1.0196	2.9206	1.6422	.40285	-2.2073	2.4850
1.9616	2.5808	1.9926	625.35	-1.6808	.9227	-2.8784	-.3179	-.8379	3.1835	1.5004	.56221	-2.0257	2.4484
2.0307	2.6627	1.8782	607.77	-1.5615	.1420	-2.3529	.0218	-.7485	3.2909	1.4830	.64096	-1.9053	2.4099
2.0438	2.6793	1.8542	604.44	-1.5358	0	-2.2545	.0790	-.7312	3.3094	1.4843	.65643	-1.8796	2.4008
Coast													
2.8482	5.5129	1.0759	604.44	1.5358	0	-1.3353	-1.8182	-.4699	3.3094	1.4843	.65643	.9541	2.4008
2.8654	5.5771	1.1038	600.05	-2.4283	.0368	-1.4924	-1.7248	-.3443	3.3338	1.4477	.62129	1.0455	2.3135
2.9000	5.6938	1.1601	591.26	-2.2687	.1254	-1.7933	-1.5039	-.1082	3.3845	1.3799	.55678	1.2236	2.3122
2.9346	5.7975	1.2152	582.47	-2.1102	.2511	-2.0794	-1.2449	.1051	3.4384	1.3216	.50005	1.3948	2.2446
2.9691	5.8905	1.2673	573.68	-1.9557	.4308	-2.3548	-.9538	.2970	3.4962	1.2750	.45040	1.5573	2.1750
3.0037	5.9750	1.3152	564.88	-1.8081	.6771	-2.6231	-.6345	.4713	3.5591	1.2418	.40622	1.7086	2.1083
3.0382	6.0531	1.3579	556.09	-1.6704	.9978	-2.8870	-.2886	.6331	3.6285	1.2230	.36532	1.8464	2.0487
3.0901	6.1617	1.4114	542.91	-1.4859	1.6250	-3.7780	.2790	.8627	3.7482	1.2222	.30493	2.0758	1.9778
3.1592	6.2972	1.4617	525.32	-1.2809	2.7326	-3.7914	1.1310	1.1678	3.9457	1.2714	.21572	2.2187	1.9204
3.2283	6.4296	1.4886	507.74	-1.1145	4.1314	-4.2859	2.1038	1.5014	4.2004	1.3749	.10637	2.3721	1.8994
3.2733	6.5172	1.4946	496.31	-1.0211	5.2038	-4.5856	2.8098	1.7485	4.4046	1.4702	.02107	2.4553	1.9037
3.2837	6.5318	1.4948	493.66	-1.0007	5.4671	-4.6511	2.9820	1.8102	4.4568	1.4954	0	0	4.8152

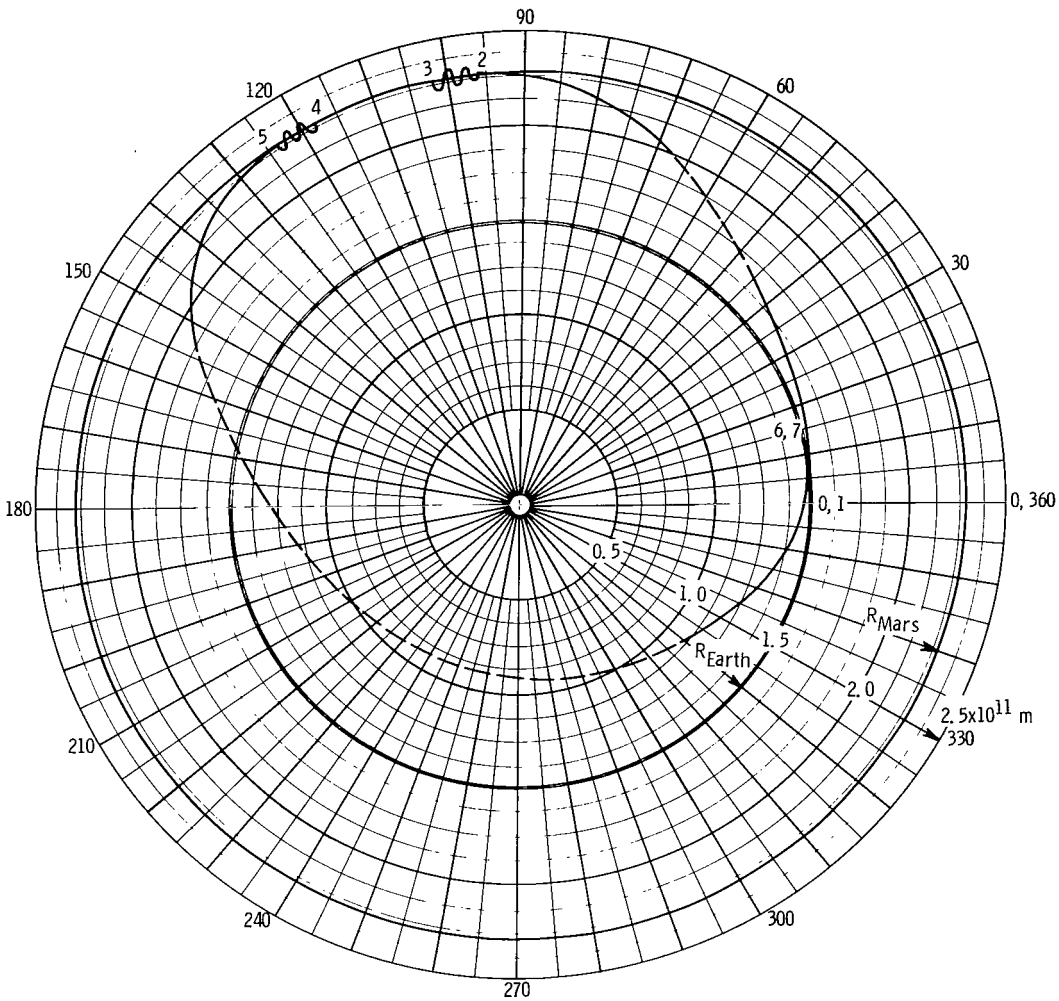

(a) Mission time, 380 days; wait time at Mars, 30 days; no initial or terminal Earth spirals; power to initial mass ratio, 100 watts per kilogram; thrust to initial mass ratio, 2.2555×10^{-3} newton per kilogram.

Figure C1. - Distance of spacecraft from Sun against angle traveled.

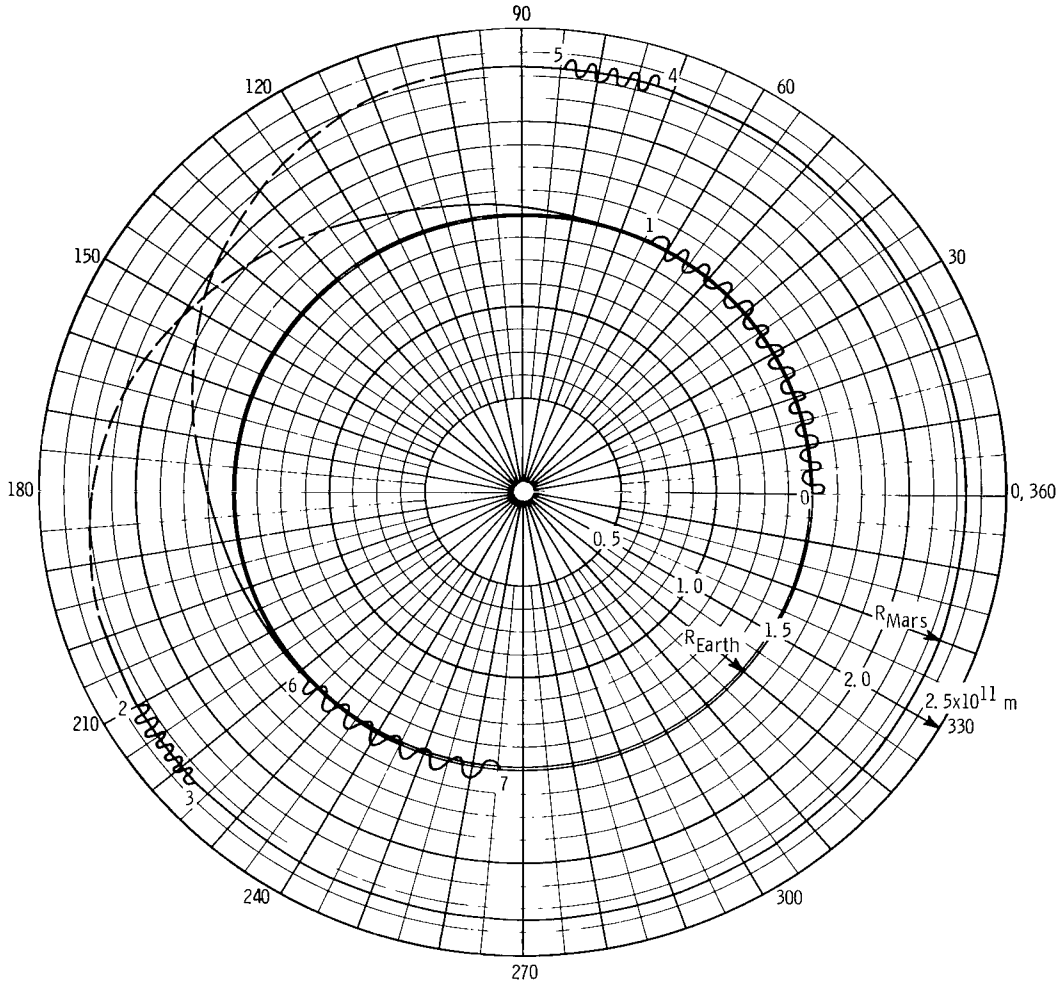

(b) Mission time, 1000 days; wait time at Mars, 400 days; 4-spiral mission; power to initial mass ratio, 55.78 watts per kilogram; thrust to initial mass ratio, 1.185×10^{-3} newton per kilogram.

Figure C1. - Concluded.

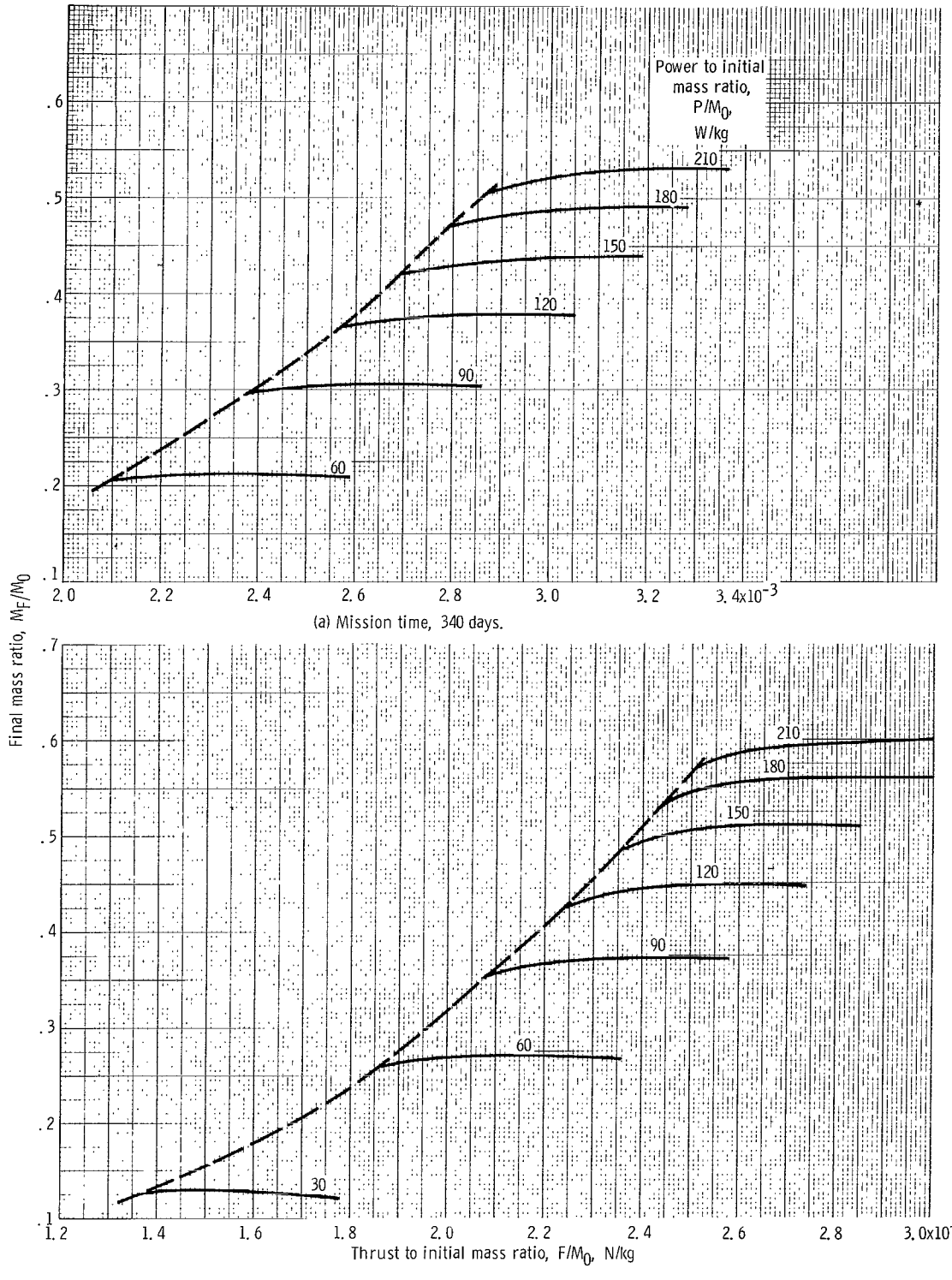

(a) Mission time, 340 days.

(b) Mission time, 380 days.

Figure C2. - Final mass ratio against thrust to initial mass ratio. Wait time, 10 days; 4-spiral mission.

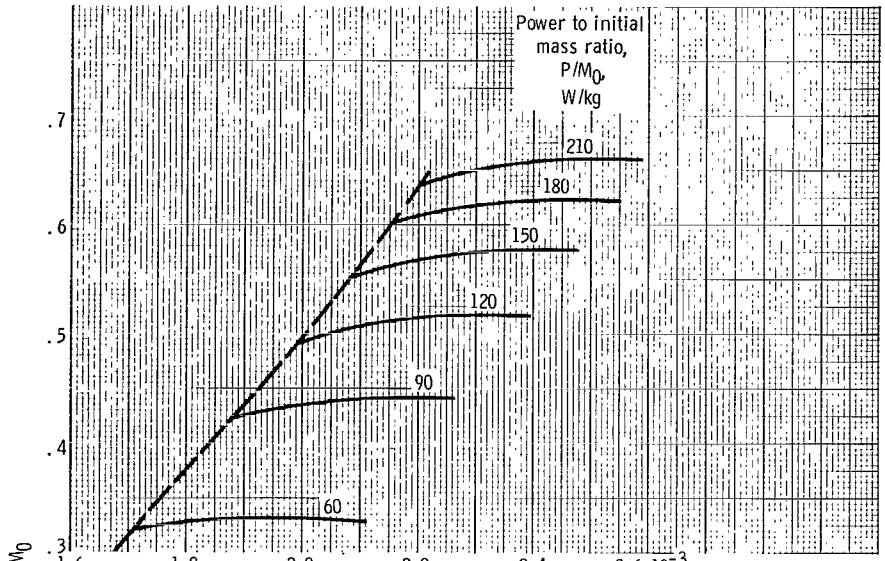

(c) Mission time, 420 days.

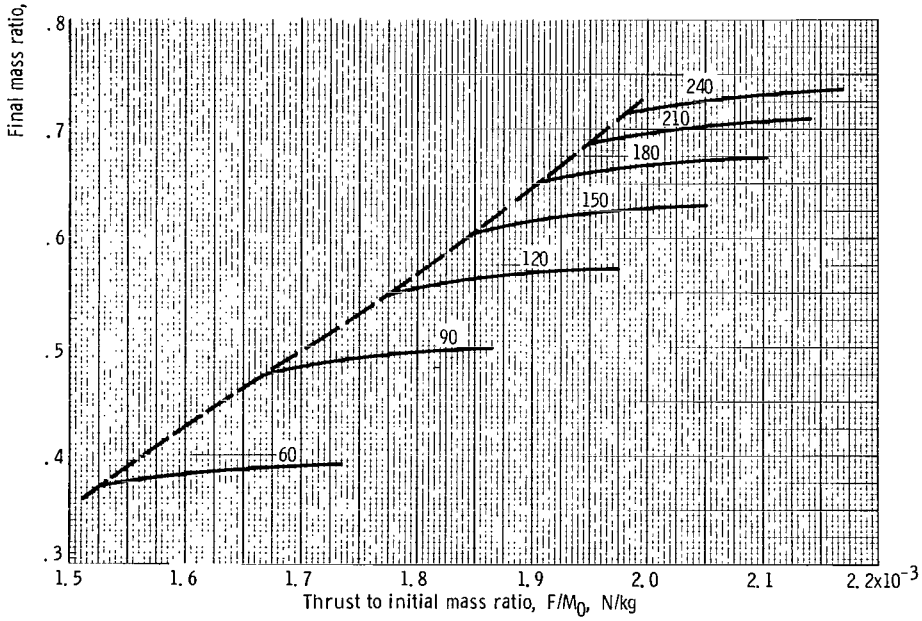

(d) Mission time, 460 days.

Figure C2. - Concluded.

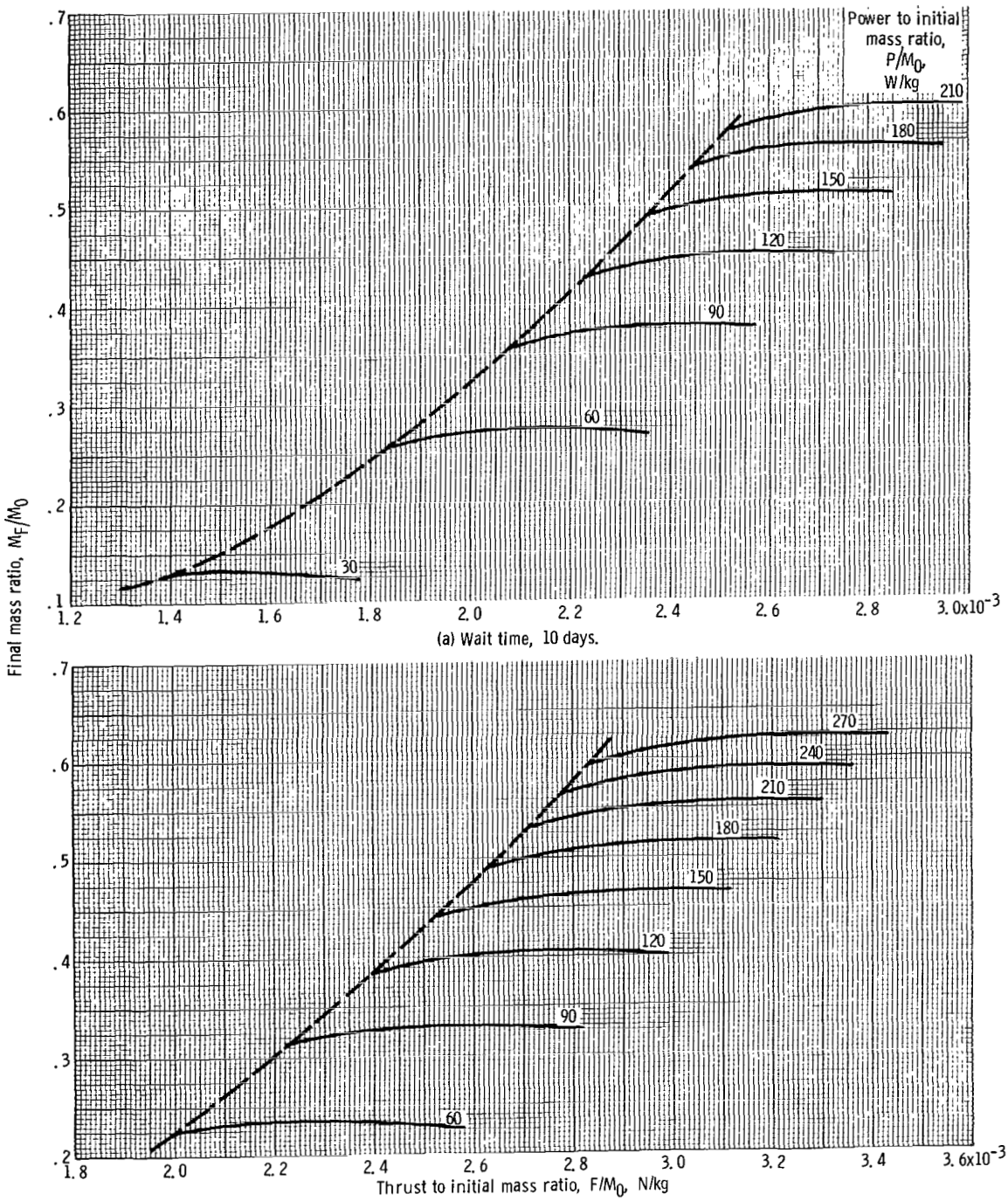

(a) Wait time, 10 days.

(b) Wait time, 30 days.

Figure C3. - Final mass ratio against thrust to initial mass ratio. Mission time, 380 days; four-spiral mission.

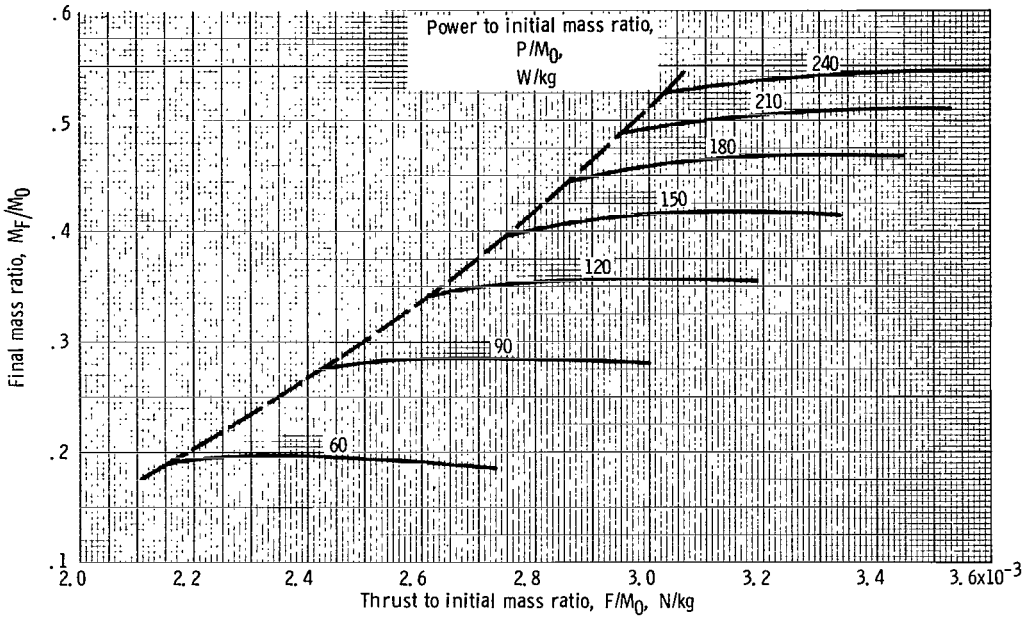

(c) Wait time, 50 days.

Figure C3. - Concluded.

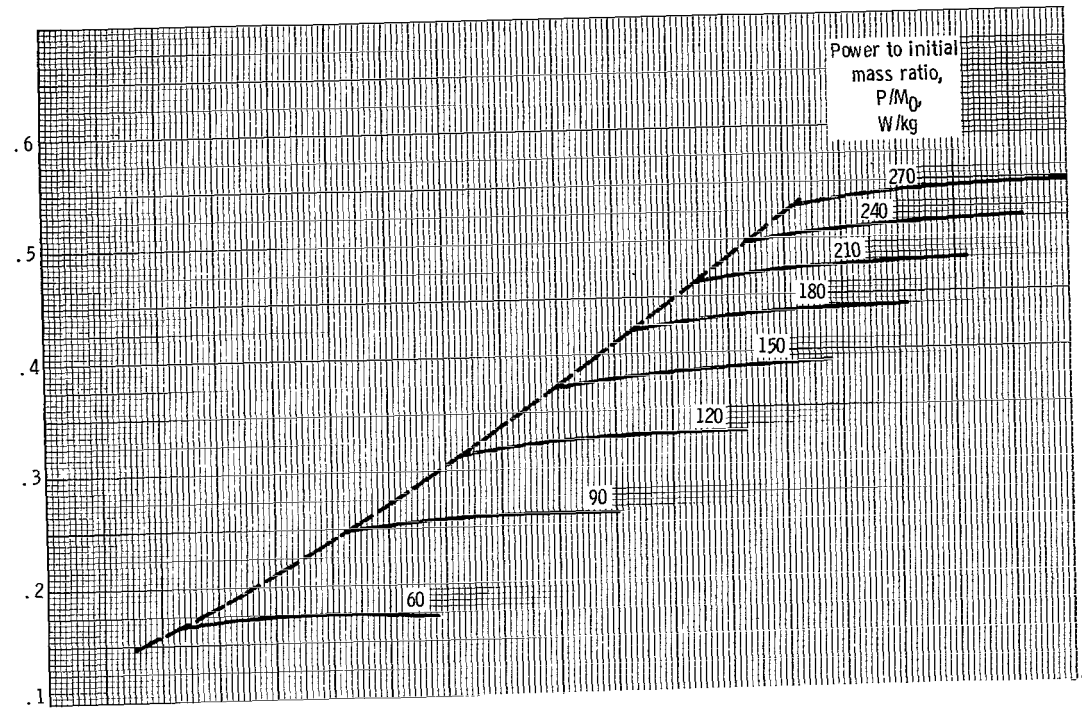

(a) Four spirals.

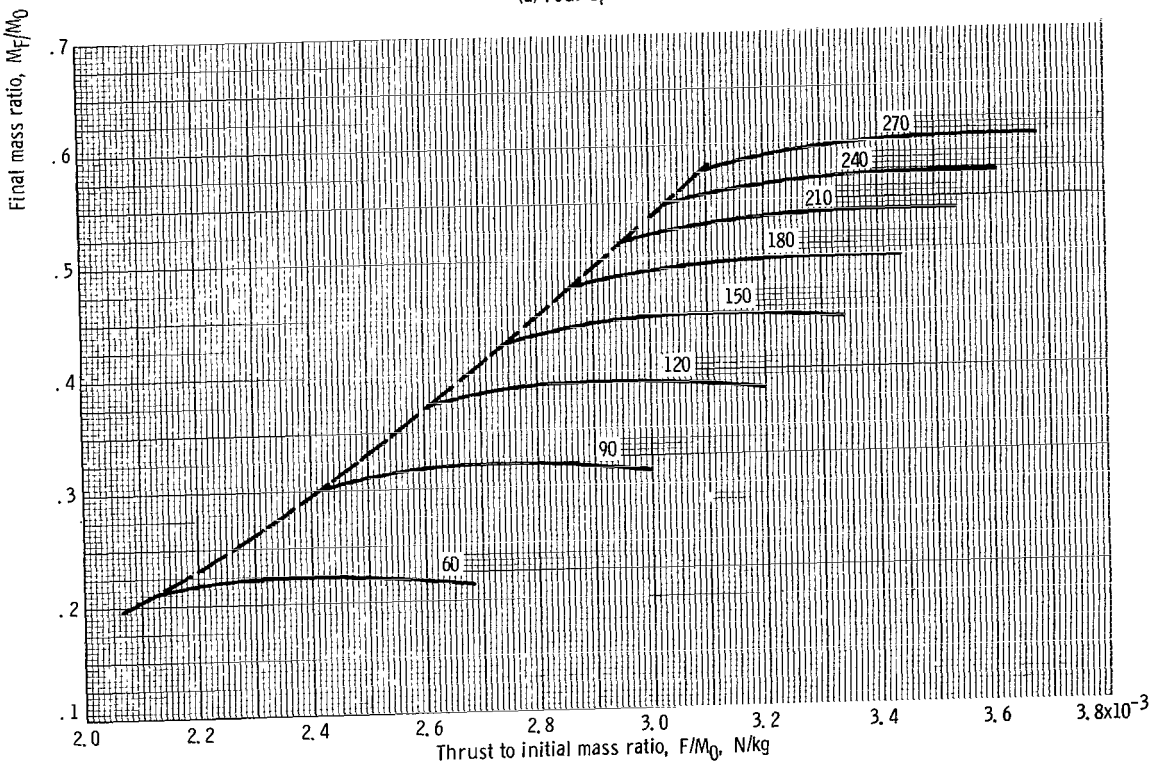

(b) No initial spiral.

Figure C4. - Final mass ratio against thrust to initial mass ratio. Mission time, 340 days; wait time, 30 days.

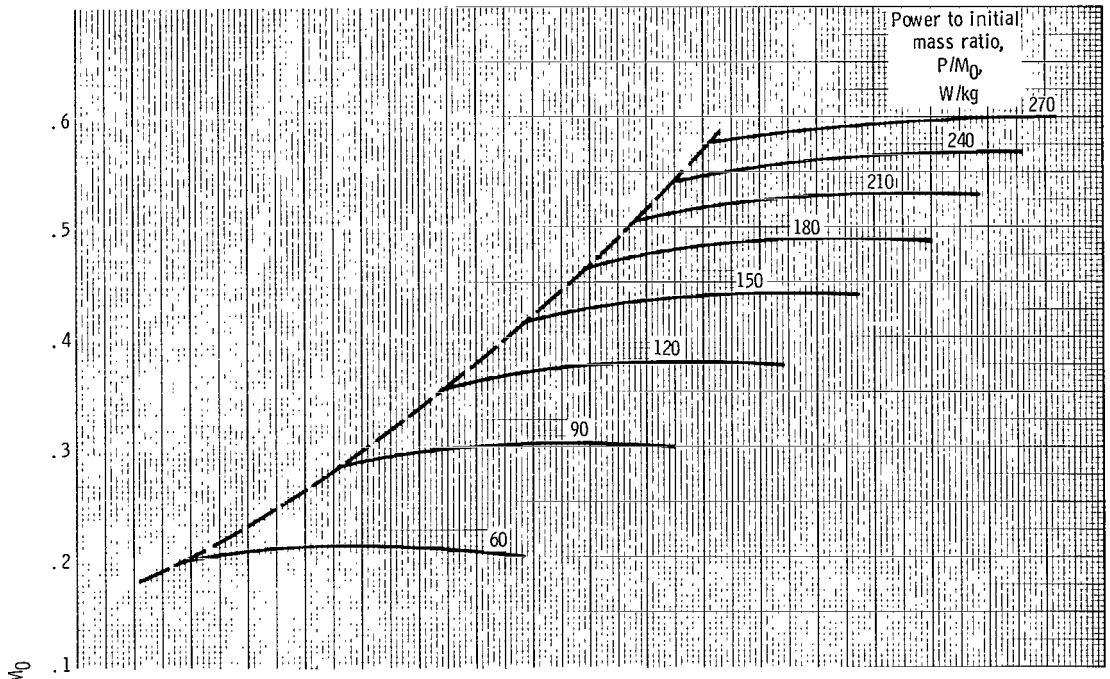

(c) No final spiral.

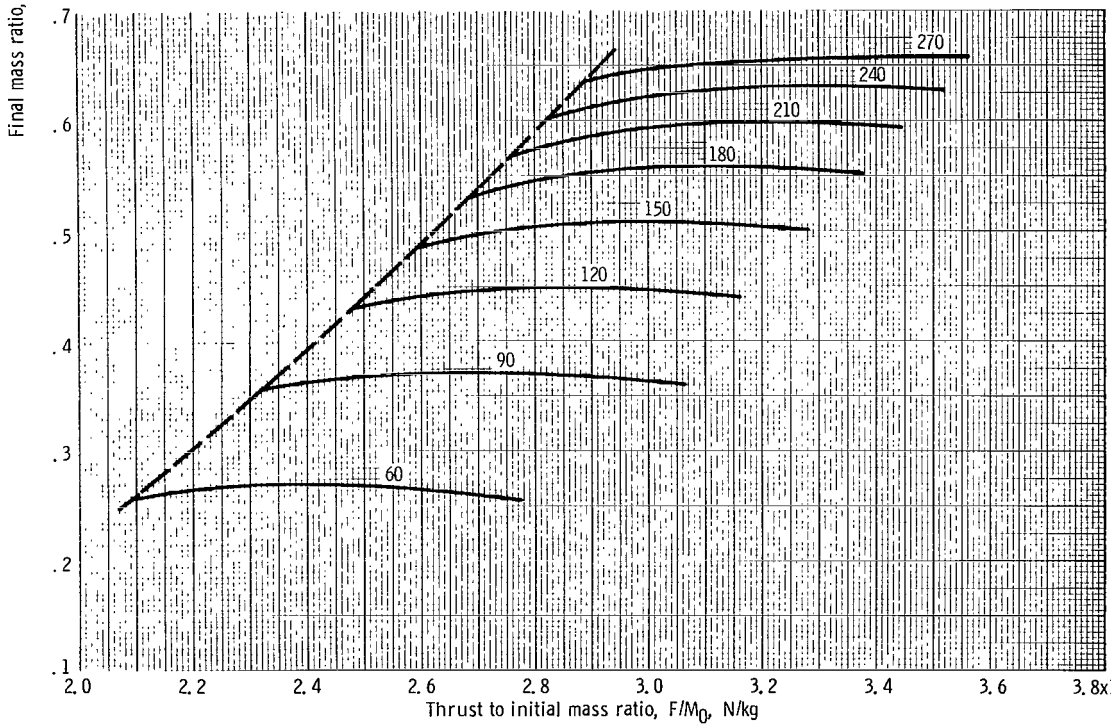

(d) No initial or final spirals.

Figure C4. - Concluded.

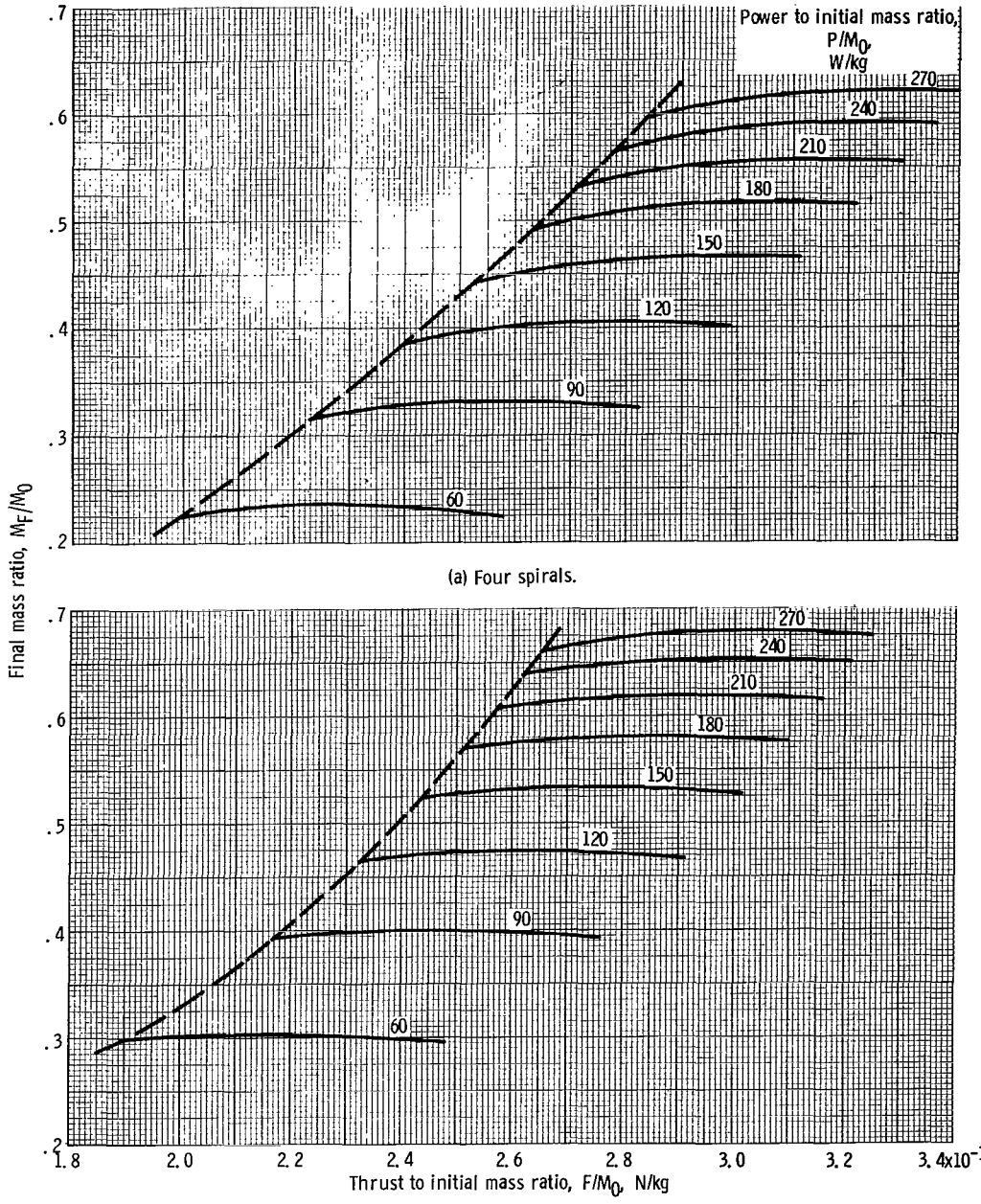

(a) Four spirals.

(b) No initial spiral.

Figure C5. - Final mission ratio against thrust to initial mass ratio. Mission time, 380 days; wait time, 30 days.

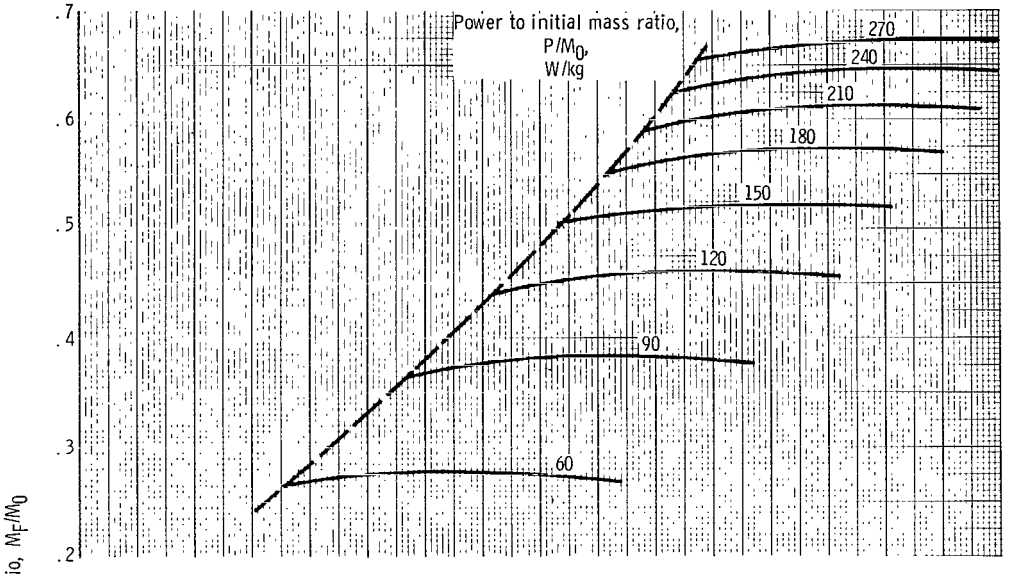

(c) No final spiral.

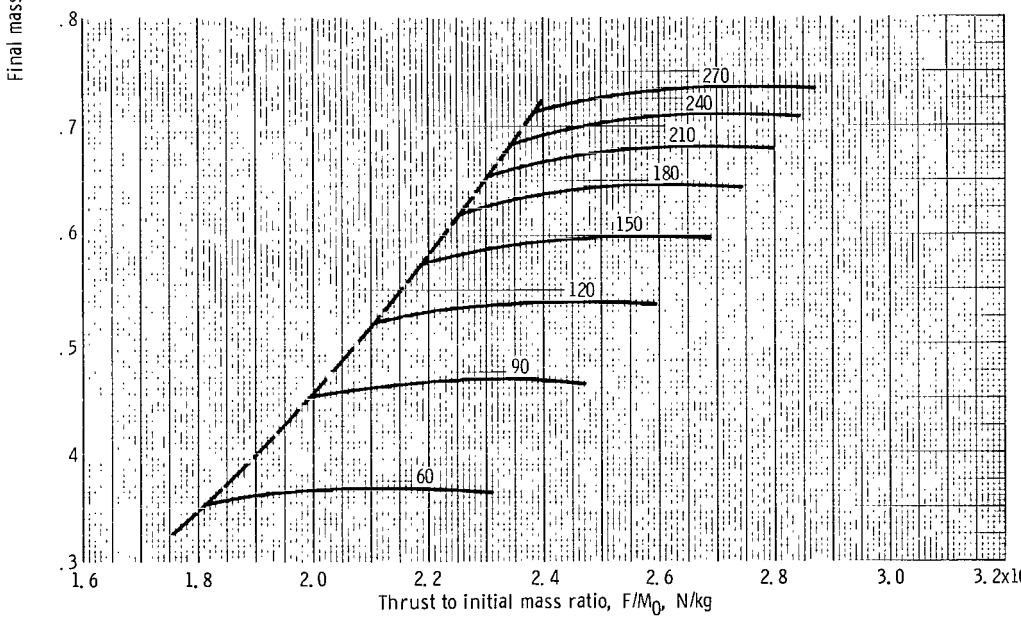

(d) No initial or final spirals.

Figure C5. - Concluded.

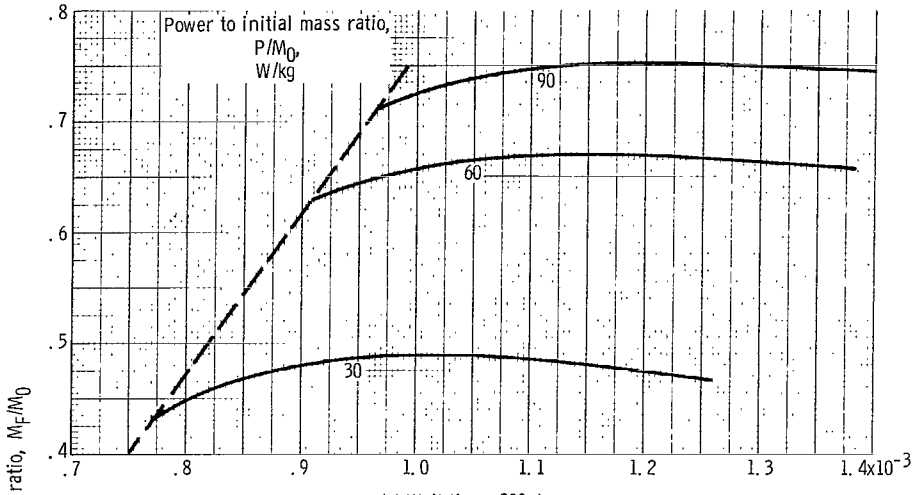

(a) Wait time, 300 days.

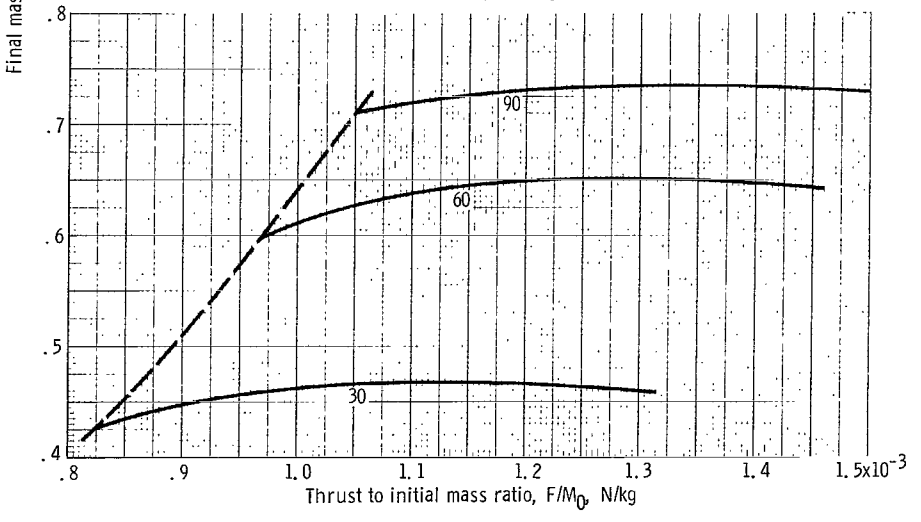

(b) Wait time, 400 days.

Figure C6. - Final mass ratio against thrust to initial mass ratio. Mission time, 1000 days; 4 spirals.

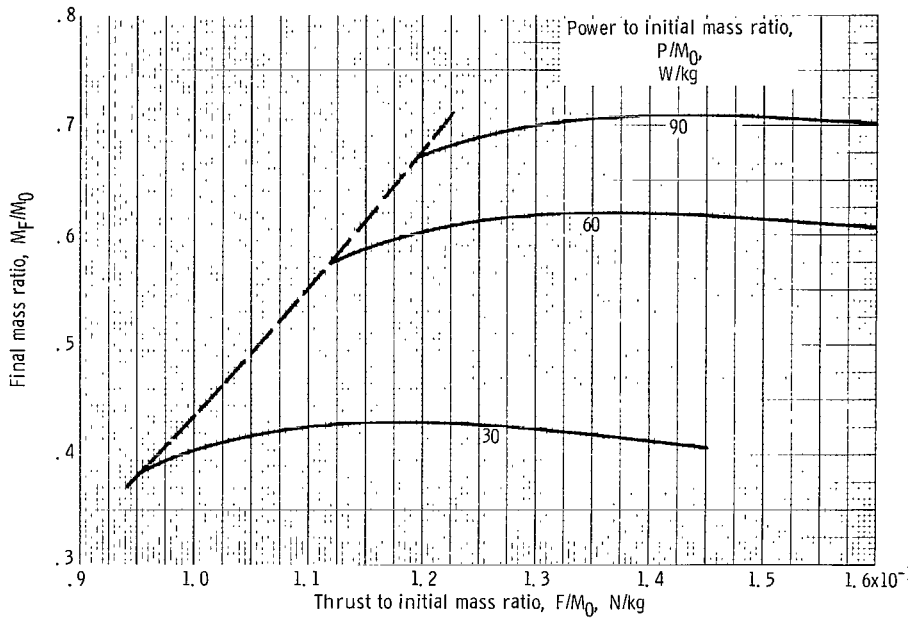

(c) Wait time, 500 days.

Figure C6. - Concluded.

REFERENCES

1. Irving, J. H.; and Blum, E. K.: Comparative Performance of Ballistic and Low-Thrust Vehicles for Flight to Mars. Vol. II of Vistas in Astronautics, M. Alperin and H. F. Gregory, eds., Pergamon Press, 1959, pp. 191-218.

2. Melbourne, W. G.: Interplanetary Trajectories and Payload Capabilities of Advanced Propulsion Vehicles. Rept. No. TR 32-68, Jet Prop. Lab., C.I.T., Mar. 31, 1961.

3. Zimmerman, Arthur V.; MacKay, John S.; and Rossa, Leonard G.: Optimum Low-Acceleration Trajectories for Interplanetary Transfers. NASA TN D-1456, 1963.

4. Moeckel, W. E.: Trajectories with Constant Tangential Thrust in Central Gravitational Fields. NASA TR R-53, 1959.

5. Sauer, Carl G., Jr.; and Melbourne, William G.: Optimum Earth-to-Mars Round-trip Trajectories Utilizing a Low-Thrust Power-Limited Propulsion System. Tech. Rept. No. 32-376, Jet Propulsion Lab., Calif. Inst. of Tech. (NASA CR-51014), Mar. 1963. (Also available as Advances in the Astronautical Sciences. Vol. 13 - Proceedings of the Ninth Annual Meeting of the American Astronautical Society, 15-17 January 1963, Los Angeles, California, Eric Burgess, ed., Western Periodicals Co., 1963, pp. 547-570.)

6. MacKay, John S.; and Rossa, Leonard G.: A Variational Method for the Optimization of Interplanetary Round-Trip Trajectories. NASA TN D-1660, 1963.

7. MacKay, John S.; Zola, Charles L.; Rossa, Leonard G.; Fishbach, Laurence H.; Strack, William C.; and Hrach, Frank J.: Manned Mars Landing Missions Using Electric Propulsion. NASA TN D-3194, 1965.

8. Lebedev, V. N.: Variational Problem of Escape from Circular Orbit. Trans. No. FTD-TT-64-1200/1+2+4, Foreign Tech. Div., Wright-Patterson Air Force Base, 1964.

9. Rossa, Leonard G.: A Parametric Study of Constant Thrust, Electrically Propelled Mars and Venus Orbiting Probes. NASA TN D-2154, 1964.

"The aeronautical and space activities of the United States shall be conducted so as to contribute . . . to the expansion of human knowledge of phenomena in the atmosphere and space. The Administration shall provide for the widest practicable and appropriate dissemination of information concerning its activities and the results thereof."

—NATIONAL AERONAUTICS AND SPACE ACT OF 1958

NASA SCIENTIFIC AND TECHNICAL PUBLICATIONS

TECHNICAL REPORTS: Scientific and technical information considered important, complete, and a lasting contribution to existing knowledge.

TECHNICAL NOTES: Information less broad in scope but nevertheless of importance as a contribution to existing knowledge.

TECHNICAL MEMORANDUMS: Information receiving limited distribution because of preliminary data, security classification, or other reasons.

CONTRACTOR REPORTS: Technical information generated in connection with a NASA contract or grant and released under NASA auspices.

TECHNICAL TRANSLATIONS: Information published in a foreign language considered to merit NASA distribution in English.

TECHNICAL REPRINTS: Information derived from NASA activities and initially published in the form of journal articles.

SPECIAL PUBLICATIONS: Information derived from or of value to NASA activities but not necessarily reporting the results of individual NASA-programmed scientific efforts. Publications include conference proceedings, monographs, data compilations, handbooks, sourcebooks, and special bibliographies.

Details on the availability of these publications may be obtained from:

SCIENTIFIC AND TECHNICAL INFORMATION DIVISION

NATIONAL AERONAUTICS AND SPACE ADMINISTRATION

Washington, D.C. 20546